COBEM 2023 27TH INTERNATIONAL CONGRESS OF MECHANICAL ENGINEERING

ABCM Brazilian Society of Mechanical Sciences and Engineering
27th ABCM International Congress of Mechanical Engineering
December 04-08, 2023, Florianópolis-SC, Brazil

COB-2023-2418
A NOVEL DESALINATION PROCESS FOR SOLAR ENERGY APPLICATIONS

Beethoven Narváez-Romo
betonarmo@usp.br
Thyago Reynaldo J. Miranda
thyago.reynaldo@outlook.com
José R. Simões-Moreira
jrsimoes@usp.br
SISEA - Renewable and Alternative Energy Systems Laboratory, Escola Politécnica at University of São Paulo, Brazil

Abstract. *Saltwater desalination is the process of obtaining fresh and drinkable water from seawater or brackish water, which requires a high degree of thermal energy due to the regular desalination process based on vaporization followed by condensation. For small and isolated communities, solar energy can be a solution to power the process. Therefore, the objective of this work is to investigate the heat transfer performance of a new desalination process using a compact two-tube configuration, where the internal tube acts as an evaporator and the external tube serves as a condenser. An experimental test rig was designed and tested in steady-state operating conditions, with experiments based on falling film technology used to vaporize water and condensate on a colder surface. Mass and energy balances were carried out for each component. Additionally, the heat transfer performance of the evaporation process was evaluated using both smooth tubes and meshed tubes. The condensation heat rate was analyzed, and it was found that the radiative heat transfer rate mechanism contributed to about 60% of the total heat transfer rate. Finally, it was noted that the operating temperature obtained in the experimental runs could be used for solar applications, and the use of solar energy as the driving power for the process could be a solution for small and isolated communities.*

Keywords: *Desalination, Solar Energy, Fresh Water, Falling film, Heat Transfer*

1. INTRODUCTION

According to the UN World Water Development Report, currently, 4 billion people experience severe physical water scarcity for at least one month per year (WWAP, 2022). Potable water resources are insufficient to meet these demands, given that only 3% of the earth's surface is drinkable, while the remaining 97% is saline (Eltawil et al., 2009). Therefore, water desalination plays a crucial role in providing access to drinking water.

Desalination technologies, such as vapor compression, reverse osmosis, multi-stage flash distillation, and multi-effect distillation are widely used in the worldwide, particularly in the Middle East and China (Xu and Dai, 2019). These technologies are energetically intensive, with a 1 m³ daily production of potable water requiring approximately 300 kWh (one tonne of oil equivalent - toe = 11.63 MWh). Nevertheless, regions with high solar irradiation potential, particularly those facing freshwater scarcity, could harness direct solar radiation exceeding 6 kWh/m² (Siddique et al., 2018).

The Brazilian semi-arid region faces a similar water vulnerability scenario as other regions of the world, with many wells containing brackish water (Grubert et al., 2014). However, this region has an advantage in terms of solar potential. Therefore, building a solar-powered desalination plant is crucial to addressing water scarcity and providing access to this essential resource for human health. The use of solar energy is not only beneficial due to its favorable geographical position and clean energy source, but also its availability, as these regions require not only water resources but also energy resources.

Desalination processes using solar energy can be classified as direct or indirect solar desalination systems. In direct systems, the solar energy collection and the distillation process occur in the same equipment, i.e. the desalination takes place in the solar energy collector. In contrast, indirect systems have two separate processes. First, the solar energy is collected by dedicated equipment and then converted into thermal energy or electricity, depending on the chosen desalination plant (Sarwar and Mansoor, 2016).

Direct solar desalination relies on the water phase change, wherein thermal energy from the Sun evaporates water, which is then condensed to produce freshwater. The main processes for direct solar desalination are solar stills (SS) and humidification-dehumidification (HD). The SS process can achieve an expected production of 4 to 5 L/m² / day, with current efficiency reaching 30 to 40% (Qiblawey and Banat, 2008). The HD process is based on the principle that wet air can contain large amounts of water vapor (Parekh et al., 2004), and as the air temperature increases, it can carry higher amounts of water vapor.

Indirect solar desalination consists of non-membrane based ones (multi-stage flash distillation, multi-effect distillation, and vapor compression) and the membrane-based (photovoltaic operated reverse osmosis and membrane distillation).

Non-membrane based technologies for indirect solar desalination include multi-stage flash distillation, multi-effect distillation, and vapor compression. In multi-stage flash distillation, the system comprises three main subsystems: heat collection, thermal storage, and multistage flash. Heat collection involves absorbing solar energy, while thermal storage (a tank) acts as a thermal damper between the heat collection system and the desalination subsystems. The desalination subsystem consists of evaporator condenser units, vacuum pump, and saltwater circulating pump, which together produce fresh water (Moustafa et al., 1985). Parabolic trough solar concentrators can be used as the heat collection subsystem (Alsehli et al., 2017). Also, solar concentrator by using simulators can be used to evaluated desalinization processes (Varón et al., 2023). The multi-effect distillation technique uses the latent heat of condensation as a multistage thermal regenerative process (Mahkamov and Akhatov, 2008). Vapor compression desalination is based on saltwater being evaporated by the heat from compressed vapor, which is then condensed (Helal and Al-Malek, 2006).

In photovoltaic operated reverse osmosis, a semi-permeable membrane is used to separate the salt ions from water, and the process occurs under external pressure by using high-pressure pumps (Al Suleimani and Nair, 2000). In membrane distillation, a membrane is used as an interface between hot salt water and the air/vapor in the membrane pores, and volatile species such as water are vaporized (Cebeci, 1974).

The evaluation of desalination equipment should consider environmental factors and ensure compatibility with solar renewable energy technologies. To this end, this work aims to investigate the heat transfer performance of a new desalination process that uses a compact two-tube configuration, with the internal tube functioning as an evaporator and the external tube as a condenser. Mass and energy balances are performed for each component, and the heat transfer performance of the evaporation process is evaluated using a smooth tube with and without mesh.

2. EXPERIMENTAL TEST RIG

The proposed design, as shown in Figure 1, consists of two concentric tubes, where the inner tube serves as the evaporator and the outer tube functions as the condenser. This configuration offers potential advantages over other designs due to its compactness. The evaporator utilizes a vertical tube falling film technology, where water is fed into the top of the tube to form a liquid film that flows down the tube. Since the evaporation process is endothermic, a secondary working fluid, also water, is heated using an electrical heater and is used to deliver the energy required for the process. The working fluid enters the bottom of the tube, creating a counter-current configuration heat exchanger.

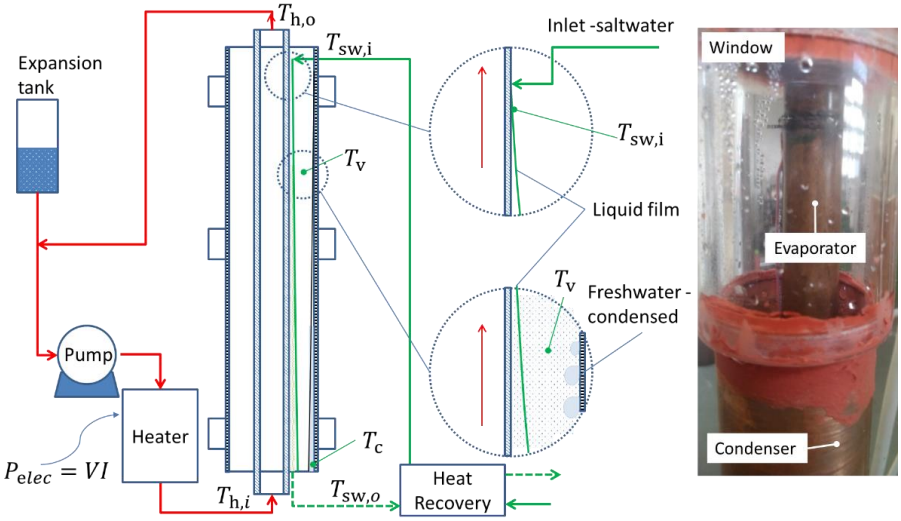

Figure 1. Schematic representation of the desalinization process

An external copper tube is installed directly as the condenser. The steam from the evaporator is directed to the internal side of the external copper tube, and the resulting heat is released to the environment through convection and radiation mechanisms, causing the steam to condense and resulting in the production of fresh water at the end of the external tube, particularly when saltwater is being used in the experimental test rig.

The experimental tests carried out in this study can be divided into two groups. The first group used a mesh (304 Stainless steel mesh, #36, 0.10 mm) on the internal tube, while the second group used a smoot tube. The experimental data obtained is presented in Table 1. The mesh installed on the external surface of the internal tube was expected to improve surface wettability. Each group consisted of four tests, in which the electrical power was controlled using a rheostat. Freshwater fluid was used instead of saltwater, and the inlet water flow was pre-heated using a heat recovery

system as shown in Figure 1. It means that the inlet water temperature was fixed as a function of the heat recovery performance.

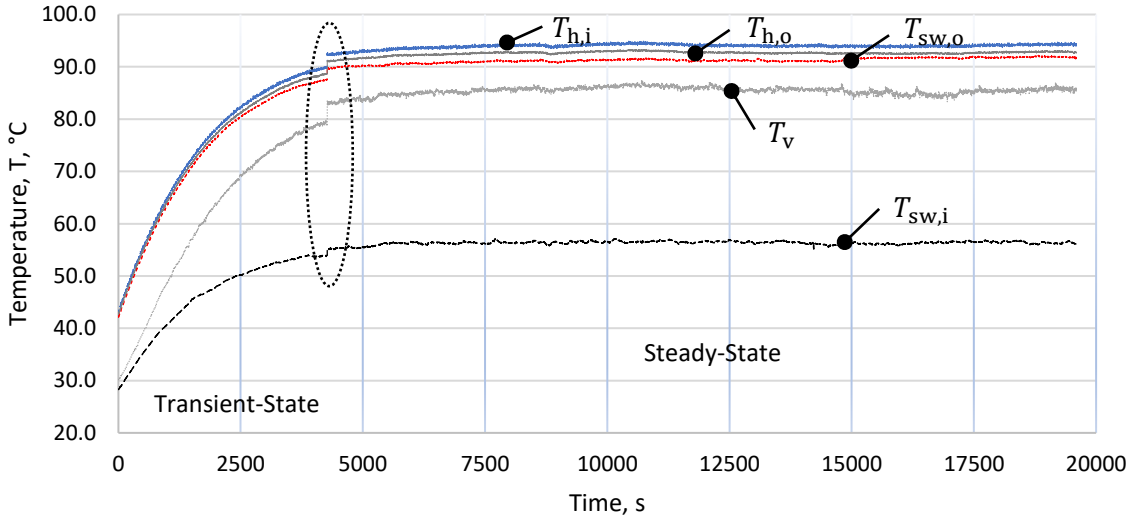

Figure 2. Temperature recording of the experimental test runs.

Table 1. Experimental set runs of the desalinization process.

Case	Heater voltage, [V]	Heater current, [Amp]	Electrical power, [W]	$T_{h,i}$, [°C]	$T_{h,o}$, [°C]	$T_{sw,i}$, [°C]	$T_{sw,o}$, [°C]	T_v, [°C]	$\dot{m}_c$, [g/s]	$\dot{m}_{sw,o}$, [g/s]
Mesh	70	7.9	553	94.1	92.7	56.4	91.8	85.2	0.0316	0.9786
Mesh	60	6.7	402	74.1	73.1	47.2	72.2	58.5	0.0205	1.0068
Mesh	50	5.6	280	64.3	63.8	41.3	62.1	53.0	0.0107	0.8382
Mesh	40	4.5	180	51.6	51.4	37.6	50.6	40.4	0.0063	1.1245
Smooth	70	7.9	553	90.4	88.9	51.8	87.4	82.2	0.0299	0.8373
Smooth	60	6.7	402	79.2	78.2	48.6	76.7	69.0	0.0193	0.7884
Smooth	50	5.6	280	64.3	63.6	42.8	62.7	50.5	0.0121	0.8535
Smooth	40	4.5	180	53.3	52.9	38.9	52.2	43.6	0.0055	1.0523

The focus of this study was to investigate the heat transfer performance of the new desalination process, and as such, each test run lasted approximately 5 hours in order to achieve a steady-state regime. Figure 2 depicts the transient and the steady-state regimes, where the latter condition was attained after 1 hour of operation. An interruption in the curve at 4200 s can be observed, which occurred because the temperature recording was stopped and restarted after the transient regime ended. During the steady-state regime, all test runs were carried out for approximately 4 hours, and the standard deviation for temperature measurements did not exceed 0.57 °C, which is equal to the temperature error of the T-type thermocouple. As shown in Figure 2, the startup of the process begins with the secondary circuit or heating circuit, which was previously turned on, explaining the initial temperature difference at the start of recording.

3. HEAT TRANSFER MODEL

The novel desalination equipment can be analyzed based on two control volumes: one for the evaporation process and the other for the condensation process, as shown in Figure 2.

3.1 Evaporator

Based on Figure 3, the mass and energy balances for control volume (CV-1) are carried out, where Eq. (1) represents the energy balance and Eq. (2) stands for the mass balance in the saltwater circuit under steady-state regime. Eq. (3) combines both equations, indicating that the energy supplied from the secondary circuit is partly used as sensible (sen) and latent (lat) heat transfer. In Eq. (1), $\dot{Q}_{rad}$ is neglected because it represents only about 3% of the total heat rate of evaporation process. Therefore, the total heat transfer ($\dot{Q}_{tot}$) in the evaporator can be obtained using Eq. (4), where $\dot{m}$ is the mass flow rate, h refers to the specific enthalpy, T is the temperature, $c_p$stands for the specific heat capacity at constant pressure, and “i” and “o” represent the inlet and outlet, respectively.

$$\dot{m}_{\mathrm{h,i}} h_{\mathrm{h,i}} + \dot{m}_{\mathrm{sw,i}} h_{\mathrm{sw,i}} = \dot{m}_{\mathrm{h,o}} h_{\mathrm{h,o}} + \dot{m}_{\mathrm{sw,o}} h_{\mathrm{sw,o}} + \dot{m}_{\mathrm{v}} h_{\mathrm{v}} \quad (1)$$

$$\dot{m}_{\mathrm{sw,i}} = \dot{m}_{\mathrm{sw,o}} + \dot{m}_{\mathrm{v}} \quad (2)$$

$$\dot{m}_{\mathrm{h}} c_{p,\mathrm{h}} \left(T_{\mathrm{h,i}} - T_{\mathrm{h,o}}\right) = \dot{m}_{\mathrm{sw,o}} c_{p,\mathrm{sw}} \left(T_{\mathrm{sw,o}} - T_{\mathrm{sw,i}}\right) + \dot{m}_{\mathrm{v}} h_{\mathrm{lv}} \quad (3)$$

$$\dot{Q}_{\mathrm{tot}} = \dot{Q}_{\mathrm{sen}} + \dot{Q}_{\mathrm{lat}} \quad (4)$$

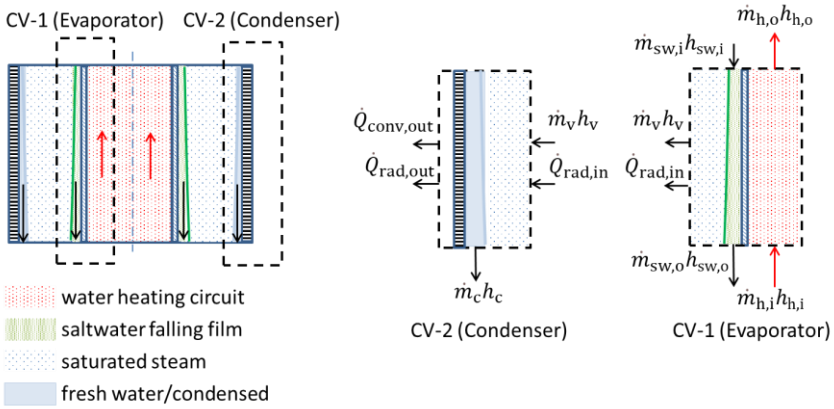

Figure 3. Control volumes of the evaporation and condensation processes for the desalinization process.

The average heat transfer coefficient of the liquid falling film (α_{f}) can be calculated by using Eq. (5), which involves heat transfer analysis in the heat exchanger. In this equation, D is the tube diameter, U is the global heat transfer coefficient, k refers to the thermal conductivity, α_{h} stands for the heat transfer coefficient in the internal flow, and f_{f} is the fouling factor (0.0002 m^2/°C W).

$$\frac{1}{\alpha_{\mathrm{f}}} = \frac{1}{U} - \left(D_{\mathrm{o}} \frac{\ln\left(\frac{D_{\mathrm{o}}}{D_{\mathrm{i}}}\right)}{2k_{\mathrm{w}}} + \frac{D_{\mathrm{o}}}{D_{\mathrm{i}}} \frac{1}{\alpha_{\mathrm{h}}} + f_{\mathrm{f}} \right) \quad (5)$$

In reference to the heating circuit's internal flow, the first step is to determine the flow regime type by calculating the Reynolds number (Re) using Eq. (6). If Re is high enough, a turbulent flow is established as it was fixed for all the tests ($\mathrm{Re_h} = 15616$), and α_{h} is defined using Gnielinski's correlation, as shown in Eq. (7). In this equation, Nu represents the Nusselt number, Pr is the Prandtl number, and f stands for the friction factor, which can be calculated as $f = (1.82 \log_{10}(\mathrm{Re_h} - 1000))^{-2}$.

$$\mathrm{Re_h} = \frac{4\dot{m}_{\mathrm{h}}}{\pi D_{\mathrm{i}} \mu_{\mathrm{h}}} \quad (6)$$

$$\mathrm{Nu_h} = \frac{\alpha_{\mathrm{h}} \phi_{\mathrm{di}}}{k_{\mathrm{h}}} = \left(\frac{f}{8}\right) \frac{\mathrm{Pr_h}(\mathrm{Re_h} - 1000)}{1 + 12.7\left(\frac{f}{8}\right)\left(\mathrm{Pr_h}^{2/3} - 1\right)} \quad (7)$$

The global heat transfer can be calculated using Eq. (8), where ΔT_{LM} is the log mean temperature difference, as defined by Eq. (9). A represents the external heat transfer area of the internal tube, with subscripts "h" and "sw" refering to the heating circuit and saltwater circuit, respectively.

$$U = \frac{\dot{Q}_{\mathrm{tot}}}{A \Delta T_{\mathrm{LM}}} \quad (8)$$

$$\Delta T_{\mathrm{LM}} = \frac{\left(T_{\mathrm{h,i}} - T_{\mathrm{sw,o}}\right) - \left(T_{\mathrm{h,o}} - T_{\mathrm{sw,i}}\right)}{\ln\left(\frac{T_{\mathrm{h,i}} - T_{\mathrm{sw,o}}}{T_{\mathrm{h,o}} - T_{\mathrm{sw,i}}}\right)} \quad (9)$$

3.2 Condenser

Condensation heat transfer occurs trough both convection Eq. (10) and radiation Eq. (11) mechanisms, with negligible thermal resistance from wall thickness conduction due to the high thermal conductivity of copper. As a result, the heat

rate of condensation ($\dot{Q}_{\text{condenser}}$) can be computed using Eq. (12). It's worth noting that the heat rate of condensation is equal to the latent heat rate of the evaporation process ($\dot{Q}_{\text{lat}}$) as defined by Eq. (13). In these equations, A refers to the external area of the external tube, $\bar{T}$ is average temperature, ϵ_{tube} stands for the tube emissivity (0.95) Narváez-Romo, (2020), and σ is the Stefan–Boltzmann constant (5.670 x 10^{-8} W/m^{2}K^4).

$$\dot{Q}_{\text{conv}} = \alpha_{\text{conv}} \cdot A \cdot (\bar{T}_{\text{w}} - T_{\infty}) \tag{10}$$

$$\dot{Q}_{\text{rad}} = \sigma \cdot A \cdot \epsilon_{\text{tube}} \cdot (\bar{T}_{\text{w}}^4 - T_{\infty}^4) \tag{11}$$

$$\dot{Q}_{\text{condenser}} = \dot{Q}_{\text{conv}} + \dot{Q}_{\text{rad}} \tag{12}$$

$$\dot{Q}_{\text{condenser}} = \dot{Q}_{\text{lat}} \tag{13}$$

The heat transfer coefficient (α_{conv}) for the vertical copper tube (external side - condenser) can be calculated using Cebeci, (1974), where the average Nusselt number for natural convection in an isothermal vertical cylinder (Nu_{tube}) is given by Eq. (14). For flat plate (fp) applications, the Churchill and Chu's (Churchill and Chu, 1973) correlation (Eq. 15) can be used to estimate the natural convection Nusselt number (Nu_{fp}). In both equations, thermal and transport properties are evaluated using the average temperature. Gr is the Grashof number, L refers to length, D is diameter, Ra is the Rayleigh number, and Pr is the Prandtl number.

$$\frac{\text{Nu}_{\text{tube}}}{\text{Nu}_{\text{fp}}} = \frac{\alpha_{\text{conv}} \cdot \text{L}}{k_{air}} = 1 + 0.3\left(32^{0.5} \cdot \text{Gr}^{-0.25} \cdot \frac{\text{L}}{D}\right) \tag{14}$$

$$\text{Nu}_{\text{fp}} = 0.68 + \frac{0.670 \cdot \text{Ra}^{0.25}}{\left(1+(0.492/\text{Pr})^{\frac{9}{16}}\right)^{\frac{4}{9}}} \tag{15}$$

4. RESULTS

4.1 Heat transfer coefficient performance in the evaporator

Figure 4 shows the heat transfer coefficients for the desalination process equipment. It should be noted that liquid falling film generally exhibits high heat transfer coefficients (Narváez-Romo et al., 2017, 2022). However, its performance is greatly influenced by hydrodynamic features, with wettability being the main challenge for this technology. The current results indicate that the liquid falling film heat transfer coefficient (Figure 4a) is lower than values reported in the open literature, which can achieve heat transfer coefficients in the range of 3000-8000 W/m^{2}K. This can be attributed to the extremely low mass flow rate used in our test runs, which exacerbates wettability issues. Recent studies have proposed methods to improve tube wettability (Narváez-Romo 2019, 2020). The global heat transfer coefficient follows the same trend (Figure 4b). Our results suggest that the main thermal resistance in the evaporation process is due to the convective heat transfer within the liquid film, as the internal flow achieves a turbulent regime.

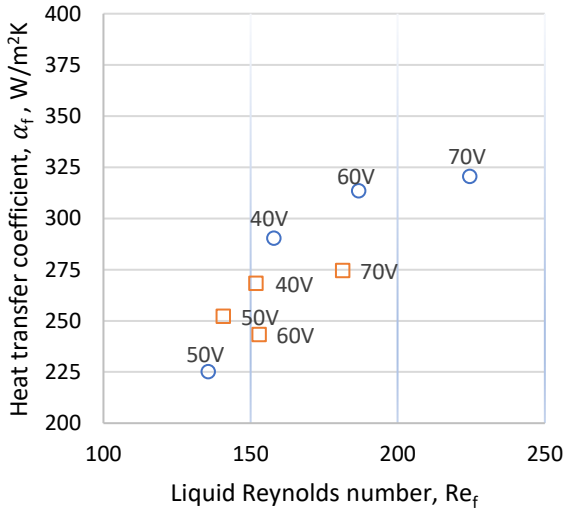

a) (○) with mesh, (▫) smooth

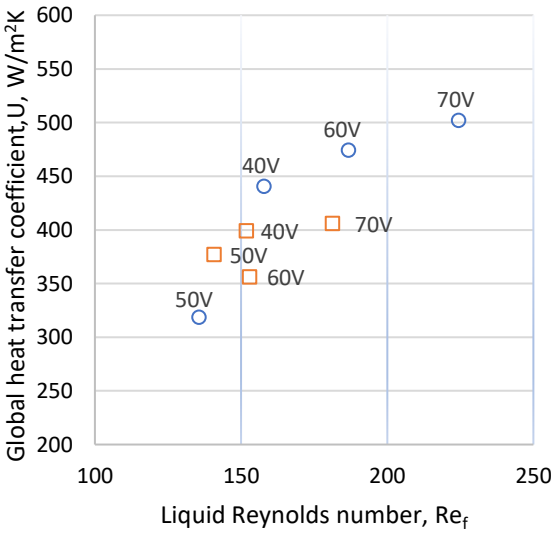

b) (○) with mesh, (▫) smooth

Figure 4. a) Average heat transfer coefficient of the liquid falling and global heat transfer coefficient of the evaporation process as a function of Reynolds number.

Moreover, the results indicate that the installing mesh on the surface tube improves the heat transfer performance. As mentioned earlier, a proper hydrodynamic distribution of the liquid film can guarantee a good heat transfer rate, with most of the tests using mesh achieving higher heat transfer coefficients than those using smooth tubes. Increasing the electrical power also promotes better performance, as the temperature difference between the liquid film and the secondary fluid increases. However, it should be noted that for 50 V, the heat transfer coefficient is lower than for other cases in the mesh setup. This may be due to wettability problems, as a Reynolds number of Re = 135 was achieved for this point. Finally, for smooth tubes, two different values of heat transfer performance were obtained for the same Reynolds number, confirming the occurrence of preferential paths for the liquid falling film.

4.2 Heat transfer coefficient performance in the condenser

The condensation heat rate was investigated using heat transfer and first thermodynamic law analyses. The results showed similar trends between the two methods. However, differences in the results can be attributed to experimental factors such as the correlation used to compute the natural convective heat transfer coefficient and experimental uncertainties, etc. Additionally, it was observed that the differences were more pronounced at 60 V when the mesh was used.

The mass flow rate of condensate increases linearly with the electrical power, as shown in Figure 5. In addition, Figure 6 displays that radiative heat transfer accounts for approximately 60 % of the total heat transfer rate during condensation. Convective heat transfer could be enhanced by utilizing forced convection with fans or implementing a finned external surface on the condenser tube.

Finally, it is worthwhile mentioning that the operating temperature obtained in the experimental runs can be achieved with solar applications by using thermal solar collectors. It should be noted that the overall process demands a high degree of thermal energy, as the regular desalination process is based on vaporization followed by condensation processes. Using solar energy as the driving power for the process could be a viable solution for small and isolated communities.

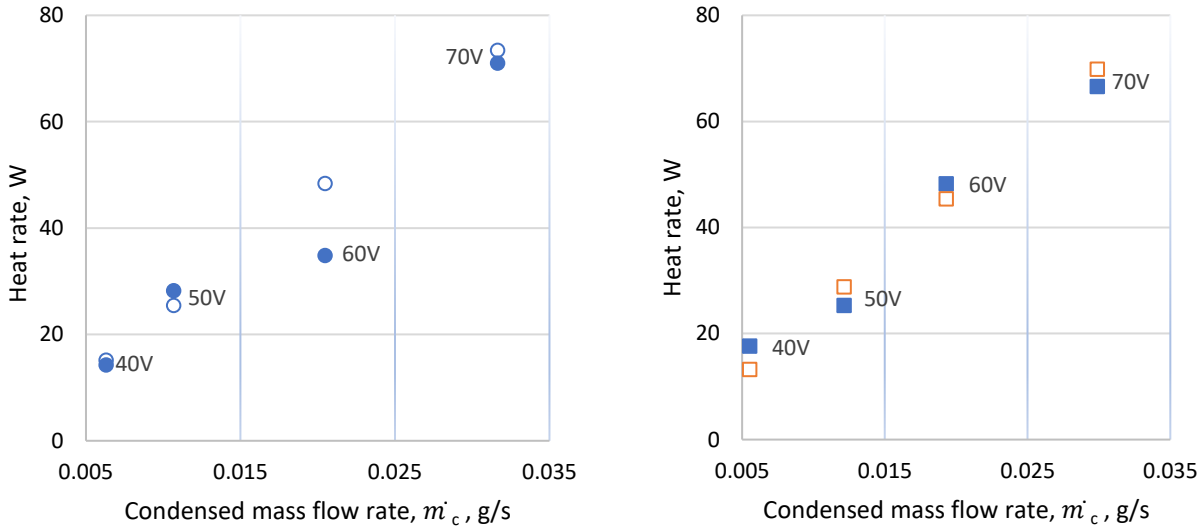

Figure 5. Heat rate of the condensation process as a function of the condensed mass flow rate. Results of $\dot{Q}_{\text{condenser}}$ - Eq. (12) are symbolized as no fill circles (○) and rectangles (▫). $\dot{Q}_{\text{lat}} = \dot{m}_{\text{v}} h_{\text{lv}}$ is symbolized as fill circles (●) and rectangles (■).

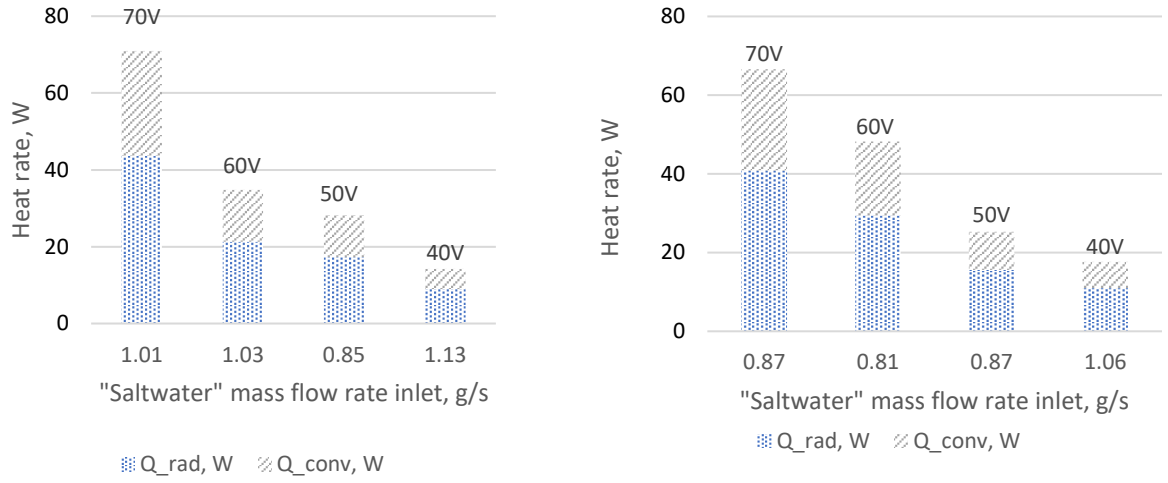

Mesh Smooth

Figure 6. Heat rate of the condensation process as a function of the condensed mass flow rate. Results of $\dot{Q}_{\text{condenser}}$ - Eq. (12) are symbolized as no fill circles (○) and rectangles (▫). $\dot{Q}_{\text{lat}} = \dot{m}_{\text{v}} h_{\text{lv}}$ is symbolized as fill circles (●) and rectangles (■).

5. CONCLUSIONS

A new approach based on vaporization followed by condensation processes for saltwater desalination was experimentally studied. Results showed that this new configuration could be a solution for small and isolated communities powered by thermal solar energy, especially in regions like Brazil with remote areas and islands with high solar incidence and lack of potable water. An experimental test rig was designed and tested in steady-state operating conditions, with experiments based on falling film technology used to vaporize water and condensate on a colder surface. Wettability problems continue to be a challenge for falling film technology, affecting the average heat transfer coefficient of the liquid film. The condensation heat rate was analyzed, and it was found that the radiative heat transfer rate mechanism contributed to about 60% of the total heat transfer rate. This suggests that the condenser could be improved in future versions by increasing the convection heat transfer coefficient or by using finned heat exchanger.

6. ACKNOWLEDGEMENTS

Authors would like to thank to the Sao Paulo Research Foundation (FAPESP) for the project funding - Grant No. 2016/09509-1. Moreover, the first author thanks Program SGA-USPSustent for the personal financial support.

7. REFERENCES

Al Suleimani, Z., Nair, V. R. “Desalination by solar-powered reverse osmosis in a remote area of the Sultanate of Oman”. *Applied Energy*, *65*(1-4), pp. 367-380, (2000).

Alsehli, M., Choi, J. K., Aljuhan, M. “A novel design for a solar powered multistage flash desalination”. *Solar Energy*, 153, pp. 348-359, (2017).

Cebeci, T. Laminar-free-convective-heat transfer from the outer surface of a vertical slender circular cylinder. In: Begel House Inc. International Heat Transfer Conference Digital Library, (1974).

Churchill, S. W.; Chu, H. H. Correlating equations for laminar and turbulent free convection from a horizontal cylinder. *International Journal of Heat and Mass Transfer*, *18*, (9), pp. 1049–1053, (1973).

Eltawil, M. A., Zhengming, Z., Yuan, L. “A review of renewable energy technologies integrated with desalination systems”. *Renewable and Sustainable Energy Reviews*, 13(9), pp. 2245-2262, (2009).

Grubert, E. A., Stillwell, A. S., Webber, M. E. “Where does solar-aided seawater desalination make sense? A method for identifying sustainable sites”. *Desalination*, 339, 10-17, (2014).

Helal, A. M., Al-Malek, S. A. “Design of a solar-assisted mechanical vapor compression (MVC) desalination unit for remote areas in the UAE”. *Desalination*, 197(1-3), pp. 273-300, (2006).

Mahkamov, K., Akhatov, J. S. “Experimental study of the performance of multieffect solar thermal water desalination system”. *Applied Solar Energy*, 44(1), pp. 31-34, (2008).

Moustafa, S. M. A., Jarrar, D. I., El-Mansy, H. I. “Performance of a self-regulating solar multistage flash desalination system”. *Solar Energy*, 35(4), pp. 333-340, (1985).

Narvaez Romo B. *An experimental study of an ammonia-water absorption refrigeration cycle using a novel modified horizontal liquid film absorption system.* Ph.D. Thesis, University of Sao Paulo, (2020).

Narvaez Romo B.; Simões-Moreira J.R. Numerical study of heat and mass transfer absorption processes using a horizontal flooded-liquid film in ammonia-water mixtures. *Proc. of the 25th IIR International Congress of Refrigeration*: Montréal, Canada, August 24-30, 2019.

Narváez-Romo, B., Chhay, M., Zavaleta-Aguilar, E. W., Simões-Moreira, J. R. A critical review of heat and mass transfer correlations for LiBr-H2O and NH3-H2O absorption refrigeration machines using falling liquid film technology. *Applied Thermal Engineering*, 123, 1079-1095, (2017).

Narváez-Romo, B., Zavaleta-Aguilar, E. W., Simões-Moreira, J. R. Heat and mass transfer in falling films technology applied to the generator and the rectifier of an ammonia-water absorption refrigeration cycle. *International Journal of Refrigeration*, 135, 276-287, (2022).

Parekh, S., Farid, M. M., Selman, J. R., Al-Hallaj, S. Solar desalination with a humidification-dehumidification technique—a comprehensive technical review. *Desalination*, *160*(2), pp. 167-186, (2004).

Qiblawey, H. M., Banat, F. "Solar thermal desalination technologies". *Desalination*, 220(1-3), pp. 633-644, (2008).

Sarwar, J., Mansoor, B. "Characterization of thermophysical properties of phase change materials for non-membrane based indirect solar desalination application". *Energy Conversion and Management*, 120, pp. 247-256, (2016).

Siddique, M., Turkmen, N., Al-Rabghi, O. M., Shabana, E., Albeirutty, M. H. "Small-scale low pressure 'single effect distillation'and 'single stage flash'solar driven barometric desalination units: a comparative analysis". *Desalination*, 444, pp. 53-62, (2018).

Varón, L.M.V., Narváez-Romo, B., Costa-Sobral, L., Barreto, G., Simões-Moreira, J.R. Novel high-flux indoor solar simulator for high temperature thermal processes, *Applied Thermal Engineering*, 2023, 121188,

WWAP, The United Nations World Water Development Report 2022: Groundwater: Making the invisible visible, UNESCO, Paris, 2022.

Xu, H., Dai, Y. J. "Parameter analysis and optimization of a two-stage solar assisted heat pump desalination system based on humidification-dehumidification process". *Solar Energy*, 187, pp.185-198, (2019).

8. RESPONSIBILITY NOTICE

The authors are the only responsible for the printed material included in this paper.